Augmenting Transmission Environments for Better Communications: Tunable Reflector Assisted MmWave WLANs

Lan Zhang, Li Yan, Bin Lin, Haichuan Ding, Yuguang Fang, *Fellow, IEEE*, and Xuming Fang, *Senior Member, IEEE*

***Abstract*—Conventional design of wireless transmissions mainly focuses on manipulating end devices to better adapt to the transmission environments, such as channel coding and modulation techniques, whose performance is significantly affected by the quality of the transmission environments. In this paper, we propose an innovative idea to proactively manipulate, reconfigure, and augment wireless transmission environments to better support end-to-end services. Specifically, we implement this idea into the commercialized millimeter-wave (mmWave) wireless local area networks (WLANs) to address the vulnerability to blockages in mmWave bands. Without damaging the aesthetic nature of environments, we deploy multiple small-piece highly-reflective metallic reflecting surfaces as tunable reflectors, where alternative indirect line-of-sight links are created by tuning the orientations of the reflecting surfaces. To demonstrate our idea, we devise a novel adaptive mechanism, *mmRef*, to enable the implementation of tunable reflectors in mmWave WLANs, where the system architecture, operational procedures, and the signaling process are developed, respectively. To theoretically quantify the expected benefits, we characterize the outage probability and system throughput of *mmRef* mechanism based on stochastic geometry theory. Simulation and numerical results demonstrate the effectiveness of implementing *mmRef* and the significantly improved system performance.**

***Index Terms*—Environment augmentation, *mmRef*, mmWave, WLAN, stochastic geometry, tunable reflector.**

Manuscript received January 10, 2020; revised March 22, 2020; accepted April 20, 2020. Date of publication April 30, 2020; date of current version July 16, 2020. This work was supported in part by the US National Science Foundation under Grant IIS-1722791. The work of B. Lin was supported in part by the National Natural Science Foundation of China under Grants 61971083 and 51939001. The work of X. Fang was supported in part by NSFC and High-Speed Rail Joint Foundation under Grant U1834210. The work of L. Yan was supported in part by the Project funded by China Postdoctoral Science Foundation under Grant 2019TQ0270. This article was presented in part at the 8th IEEE/CIC International Conference on Communications in China, Changchun, China, August 11–13, 2019. The review of this article was coordinated by Dr. L. Zhao. *(Corresponding author: Yuguang Fang.)*

Lan Zhang and Yuguang Fang are with the Department of Electrical and Computer Engineering, University of Florida, Gainesville, FL 32611 USA (e-mail: lanzhang@ufl.edu; fang@ece.ufl.edu).

Li Yan and Xuming Fang are with the Key Laboratory of Information Coding and Transmission, Southwest Jiaotong University, Chengdu 610031, China (e-mail: liyan12047001@my.swjtu.edu.cn; xmfang@swjtu.edu.cn).

Bin Lin is with the School of Information and Communications Engineering, Dalian Maritime University, Dalian 116026, China (e-mail: binlin@dlmu.edu.cn).

Haichuan Ding is with the Department of Electrical Engineering and Computer Science, University of Michigan, Ann Arbor, MI 48109 USA (e-mail: dhcbit@gmail.com).

Digital Object Identifier 10.1109/TVT.2020.2991547

I. Introduction

WIRELESS communication has served as the linchpin of modern society since the invention of the telegram. In the last few decades, great efforts have been put on enhancing wireless communication performance. Due to the uncertainty of wireless environments, most existing design focuses on manipulating end devices, i.e., transmitter and receiver, to adapt to the transmission environments for better communications, such as channel coding, modulation, and power management techniques [2]–[4].

However, their transmission performance might be seriously affected or limited by the quality of the transmission environments. For example, beamforming techniques have been widely used in millimeter-wave (mmWave) communications to address the severe signal attenuation due to the short wavelength [4], [5]. However, even with an accurate beam alignment, an mmWave link can be easily interrupted by the dynamic transmission environments like a moving human body, due to the poor penetration and diffraction, as well as the nature of directional transmissions in mmWave bands [4], [5]. Unfortunately, the interruption can be hardly avoided by enhancing end devices, such as increasing transmit power or directivity gain. Motivated by such observations, in contrast to only manipulating end devices, this paper seeks a novel way to proactively manipulate, reconfigure, and finally augment mmWave transmission environments. To demonstrate our idea, we focus on mmWave wireless local area networks (WLANs), the frontier of the commercialized mmWave communications [6]–[8], to address the vulnerability of blockages for better mmWave WLANs.

Recently, increasing attention has been put on taking transmission environments into account for better mmWave communications [9]–[11]. Through bouncing off surrounding environments like wall and floor, Xue *et al.* proposed to concurrently transmit multiple reflected beams to one user [9]. However, the reflection loss caused by the poor reflectance of surrounding environments was not considered, where the attenuation can be almost 40% through reflecting by materials like drywall [12], [13]. Fortunately, smooth metallic plates with perfect reflectance, i.e., reflecting nearly 100% signal strength [10], can be deployed cost-effectively to guarantee the quality of reflected signals. Zhou, *et al.* deployed a metallic ceiling in a data center to enable the simultaneous transmissions of multiple machine pairs

through mmWave bands, whose effectiveness is verified through the testbed [10]. Similar idea was used in a multi-cubicle office for simultaneous mmWave transmissions [11]. However, unlike a data center used to hold multiple computing servers, WLANs are usually used by human beings and the coverage areas tend to be inhabited by people, where fully metal-coated ceiling may lead to inconvenient and unattractive living environments. Therefore, we propose to implement multiple small controllable (smart) reflectors in order to collaboratively manipulating WLAN transmission environments without damaging the aesthetic nature.

Considering the unpredictable transmission outages caused by the varying environments, e.g., a static user station (STA) blocked by dynamic obstacles, as well as the limited coverage of a small-piece metallic plate,[1] we incorporate controllable angle tuning function into the reflector design. In this way, the transmission environment can be reconfigured by flexibly tuning the angles of multiple reflector plates to effectively adapt to the varying WLAN transmission environments. As a remark, we must point out that the angle tuning may take time and mechanical energy, and thus the environment augmentation is designed to be user oriented in the sense that the environmental augmentation with reflectors depends on the current user configuration and the applications demanded by the users. For example, the requester can be a blocked STA with a relatively long remaining service time, where the sacrificed angle tuning overhead is worthwhile for the continuous transmissions through reflective links. Thus, the reflector angle adaptation must be done according to certain criterion. Our recent work devised the criterion for augmenting vehicular transmission environments [14]. In addition, it should be mentioned that besides the mechanically tunable metallic surface, the entity of reflectors can also be chosen as the reflector-array or reconfigurable meta surface [15], [16]. This paper implements the former tunable metallic surface as an example of reflectors to demonstrate our idea. To the best of our knowledge, none of existing research has considered to proactively augment mmWave WLAN transmission environments by collaboratively and flexibly manipulating multiple tunable reflectors.

In this paper, we propose to proactively manipulate, reconfigure, and finally augment the transmission environments of mmWave WLANs without damaging the aesthetic nature. By deploying relatively cheap reflectors (comparing with regular mmWave communication devices), the communication quality is boosted by dynamically tuning the angles of reflecting surfaces. As a proof of concept, this paper serves as the first step towards this goal. We focus on two fundamental questions: How to implement the tunable reflectors in WLANs? What performance benefits can be expected? Our main contributions are summarized as follows:

- We propose a novel adaptive mechanism, called *mmRef*, to effectively implement tunable reflectors in mmWave WLANs. The system architecture is developed from the control-/data-plane decoupling design [17], [18]. Considering the inherent blindness of directional transmissions, a controller operating at the relatively reliable low-frequency bands is introduced with omni-directional coverage, supporting fast handshakes among the transmitter (Tx), relaying reflector(s) and receiver (Rx), and facilitating directional mmWave transmissions.
- We design the operational procedures of *mmRef* to enable indirect LoS reflective links. The signaling process and two algorithms are designed to ensure the performance of establishing reflective links.
- Based on the stochastic geometry theory, we theoretically evaluate the expected performance by implementing *mmRef*. Specifically, we characteristic the outage probability and throughput of reflective transmissions. Unlike the channel model for a direct link, the characterization of a reflective link is challenging because we have to consider both Tx-reflector and reflector-Rx links.
- Based on extensive simulation and numerical experiments, we have demonstrated the effectiveness of the proposed *mmRef* implementation. Meanwhile, the benefits in terms of the outage and throughput performance are significant in the augmented mmWave WLAN environment.

[1] Based on the strict reflection rule (identical incidence and reflection angle), a reflector with static orientation can only serve STAs in very limited area.

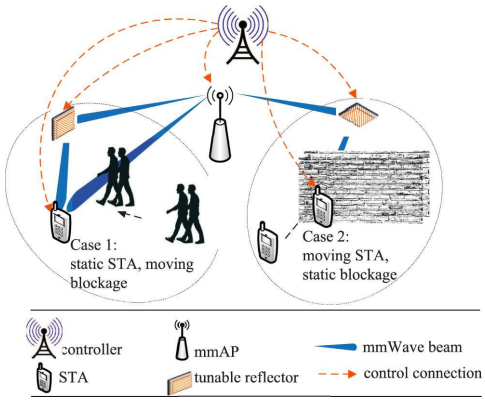

Fig. 1. The system architecture of *mmRef* for tunable reflector enabled transmission environment augmentation in mmWave WLANs.

The rest of this paper is organized as follows. Section II presents the overview of *mmRef*. Section III details system operation procedure and the smart reflective-link establishment scheme. Section IV theoretically analyzes the system performance. Simulation and numerical results are evaluated in Section V. Section VI concludes this paper.

II. Overview of mmRef Mechanism

To implement tunable reflectors in mmWave WLANs, we propose a novel adaptive mechanism, *mmRef*. In this section, we first present the system architecture of *mmRef*, followed by its advantages.

A. The System Architecture

To automatically mitigate the inherent blindness of directional transmissions while saving cost, we develop the system architecture from the concept of control-/data-plane decoupling [17], [18]. As shown in Fig. 1, the whole system is composed of mmWave access points (mmAPs), a controller, tunable reflectors

and STAs. The data-plane provides mmWave services with up to multi-Gbps data rate by mmAPs. The control-plan aims at fast handshakes among Tx, relaying reflector(s), and Rx, facilitating operations on directional mmWave transmissions, which is assumed to be reliable based on the advanced technologies in cyber-physical systems nowadays. The control-plane is coordinated by a controller, which could physically be a legacy AP using relatively reliable low-frequency bands with omni-directional coverage.[2] Based on the control signalling, the angle of a reflector plate can be adjusted to tune the reflected beam to optimally serve surrounding STAs. This work utilizes multiple reflector plates with tunable functions. Each tunable reflector is composed of a cheap metallic plate, such as aluminium sheets [10], [19], a low-frequency transceiver and a simple mechanical device. Instead of the more expensive mmWave transceivers, cost-effective low-frequency transceivers, such as the commercialized WLAN transceivers at 2.4 GHz band, are used. The mechanical/electrical device is equipped to control the metallic plate. As aforementioned, the entity of tunable reflectors can also be the reflector-array or intelligent reconfigurable meta-surfaces [15], [16]. To enable the reflective link between an mmAP-STA pair, the controller connects with mmAPs through either low-frequency links or deployed wired links, depending on specific applications. An STA equips both the low-frequency and mmWave transceivers for control-/data-plane signaling, respectively. It should be mentioned that the reflector placement is another interesting research problem, especially for different WLAN environments like offices and malls, which is out of scope of this work. This work assumes that tunable reflectors are already placed in WLAN environments, and the optimal placement will be explored in our future work.

B. Why mmRef?

The idea of utilizing reflected beams has already been incorporated in IEEE 802.11ad standard [6], [20], [21]. Based on exhaustive search, the beam with the strongest received signal strength is selected, which might be the superposition of reflected signals especially when the direct link is blocked. However, outages still happen due to the severe attenuation impinging on normal surrounding environments [12], [13], [22]. As illustrated in Fig. 1, the interrupted transmissions are usually caused by the unpredictable changes in the environment, which can be roughly divided into two cases: the moving obstacle blocks a static STA or the moving STA encounters static blockages. As aforementioned, considering the time and energy overhead of reflector angle tuning, this work focuses on devising *mmRef* mechanism for interrupted individual STAs with large-scale remaining transmissions, where the sacrificed overhead is worthwhile for their continuous transmissions through reflective links. This is particularly suitable in WLANs as a user tends to stay at a location stationary for relatively long time for his/her services. To reconfigure the transmission environments for optimal service deliveries for all users under the coverage seems to provide a viable solution. In addition, the *mmRef* architecture can be adopted to serve other application scenarios. For example, a system operator can reconfigure the overall transmission environment to circumvent possible blockages at a larger time scale. Due to the page limit, other application scenarios will be explored in our future work. In summary, the *mmRef* system architecture has the following advantages:

- *Compatible:* The *mmRef* changes beam directions in the middle of propagation, which can be used for different mmWave WLAN standards.
- *Flexible and expandable:* The deployment of tunable reflectors can be dynamically changed based on specific scenarios, such as crowded or sparse, indoor or outdoor. Moreover, the centralized control can flexibly realize diverse system goals, such as maximizing system throughput, minimizing blind spots, etc.
- *User-oriented:* The *mmRef* is an option for STAs in mmWave WLANs, i.e., an STA may not use mmRef when transmission interruptions in the environment are not too many.
- *Cost-effective:* Besides the lower cost of a tunable reflectors compared with a mmWave relay, the forwarding energy of relays can be further saved in the established reflective links, especially for a long-term transmission.

III. The MmRef Implementation

Based on the system architecture, this section first elaborates the corresponding operational procedures, followed by a reflective link establishment scheme.

A. Operational Procedures

We design the operational procedures into two modules, namely, *Initialization Module* and *Service Module*. The initialization module periodically acquires the information of serving devices, i.e., mmAPs and reflectors, based on which the service module provides mmWave transmissions through reflective links. In the following, we detail the operations in the two modules, respectively.

1) As illustrated in Fig. 2, the *Initialization Module* first generates the topology of all serving devices. Specifically, based on the location of mmAP n, the controller records the locations of all applicable reflectors for mmAP n through a table T_n, named by *MTable*. Instead of simply recording, T_n is a two-dimensional table with size $M \times J$, where each table element records information of one reflector, including its identity (ID), location, and usability (either idle or occupied). M and J represents the number of all beam directions of mmAP n and the maximal considered reflectors in one beam direction, respectively. Note that IEEE 802.11ad standard divides the 360° omnidirectional space into a set of equal-size consecutive sectors $S = \{S_1, S_2, \ldots, S_M\}$, where each sector corresponds to a beam direction with beam-width θ^{mmAP}, and $\theta^{mmAP} \times M = 360°$. To adapt our reflective links to the directional transmissions based on IEEE 802.11ad standard, we record reflectors geographically located in different sectors into different rows, where reflectors in the ith row of T_n are located inside the

[2] Note that the controller can be a software or firm ware. For example the controller can be implemented at a base station in cellular systems, if WLANs and cellular systems are integrated.

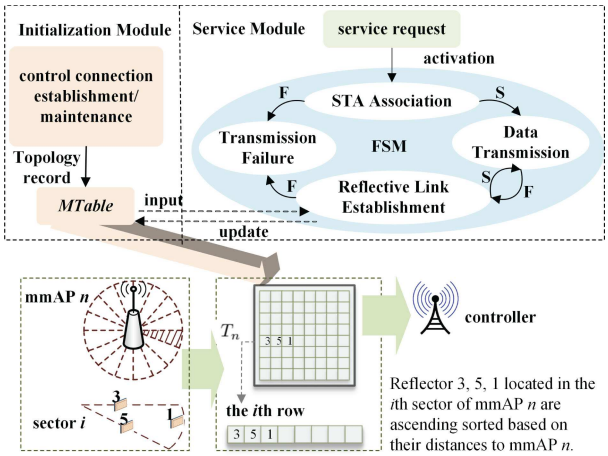

Fig. 2. The operation procedures of *mmRef*. Note state transition condition S and F respectively represent succeed and failed output.

ith sector of mmAP n. In addition, considering the severe distance-related propagation loss, with unknown STA locations and unpredictable blockages, a reflector geometrically closer to an mmAP is preferred due to the average better transmission performance brought by geometric proximity, which will be further discussed later. Thus, to better utilize deployed reflectors, the reflectors in the row of T_n are sorted in an ascending order based on their distances to mmAP n. As an example in Fig. 2, reflector 1, 3 and 5 are located inside sector i, and reflector 3 is the geometrically closest one to mmAP n.

2) The *Service Module* is operated based on a finite machine state (FSM) that is activated due to the *mmRef* service request sent from an STA. The FSM includes 5 states that are detailed below.

- In STA association state, an STA respectively connects to the controller and an mmAP based on existing WLAN standards, where the two associations can respectively refer to IEEE 802.11ad standard and IEEE 802.11 g standard when the controller is a 2.4 GHz AP [6], [7], [20], [23].
- In data transmission state, high-speed data services are provided by mmAPs through either the established direct or reflective links, or the links based on IEEE 802.11ad standard [6], [7], [20], [23].
- Both the transmission failure and data transmission states can terminate this FSM, and the corresponding feedback is sent back to the STA.
- The reflective link establishment state is the core of the FSM, which is activated due to the transmission interruption, i.e., the failure of data transmission state. This state aims to select available reflectors and their corresponding angles to recover the interrupted transmission. To efficiently and effectively manage this state, we design a reflective link establishment scheme detailed below.

B. Reflective Link Establishment Scheme

As the critical state of the service module, the overhead of this state determines the delay of the transmission recovery from outage. Meanwhile, the selected reflectors and the corresponding tuned angles determine the quality of the reflected signal. Thus, we first design the signaling process, followed by two algorithms for this state.

1) Signaling Process: As illustrated in Fig. 3, the signaling process is activated due to the transmission interruption of STA i, where a service request as well as the information of the serving device is sent to the controller in signalling 1). Signaling 1) carries the identity of the associated mmAP and the previous transmission sector S_i^n. Based on signaling 1), the controller sends an inquiry to mmAP n in signaling 2) to examine its serving ability.[3] Once the service can be continuously provided by mmAP n, based on signaling 3), the controller sends back an acknowledgement (ACK) to STA i in signaling 4) and selects reflectors based on Algorithm 1 (smart reflector candidate selection, SRCS) detailed later. Denote the reflector set participating the following angle tuning between mmAP n and STA i by reflector candidates RC_i^n, where RC_i^n is derived by Algorithm 1. The controller informs the selected RC_i^n to start reflector angle tuning (RAT) in signaling 5). Once ACKs are sent back from these reflectors in signaling 6), the controller assigns them to mmAP n in signaling 7). After acquiring beam directions pointing at RC_i^n, an ACK is sent back from mmAP n in signaling 8). The controller coordinates mmAP n, STA i and reflector candidates RC_i^n for synchronization in signaling 9), and then operates the Algorithm 2 (fast reflector angle tuning, FRAT) detailed later for RAT. Based on the outputs including serving reflector identity RI_i^n and their corresponding angle RA_i^n, the controller respectively informs mmAP n, STA i and RI_i^n in signaling 10). Once the ACKs are received in the controller in signaling 11)-13), the data transmission through a reflective link is established.

Note that the overhead of the aforementioned control signaling transmissions is usually very limited, since the light payload of control signaling leads to short transmission time and robust transmission mechanisms, such as the reliable channel coding and modulation schemes. Rather than waiting for the unpredictable transmission recovery as shown in Fig. 1, *mmRef* provides a solution to create the recovery while sacrificing the overhead for the reflective link establishment. To capture the channel variation, these reflective links should be trained within the beam coherence time, which is defined to characterize the frequency of beam alignment in directional mmWave transmissions [24]. Although the beam coherence time in low-mobility short-range WLANs is further increased compared with that (a few seconds based on simulations in [24]) in highly dynamic vehicular environments, reflective links should be fast established to guarantee the system performance. Therefore, the SRCS and FRAT algorithms are respectively proposed to accelerate the reflective link establishment while guaranteeing the link performance.

2) Smart Reflector Candidate Selection (SRCS): Due to the tunable design, all reflectors surrounding an mmAP can be

[3]The reason that serving ability of an mmAP is checked is to avoid the outage due to the inability of the mmAP to support the requested service.

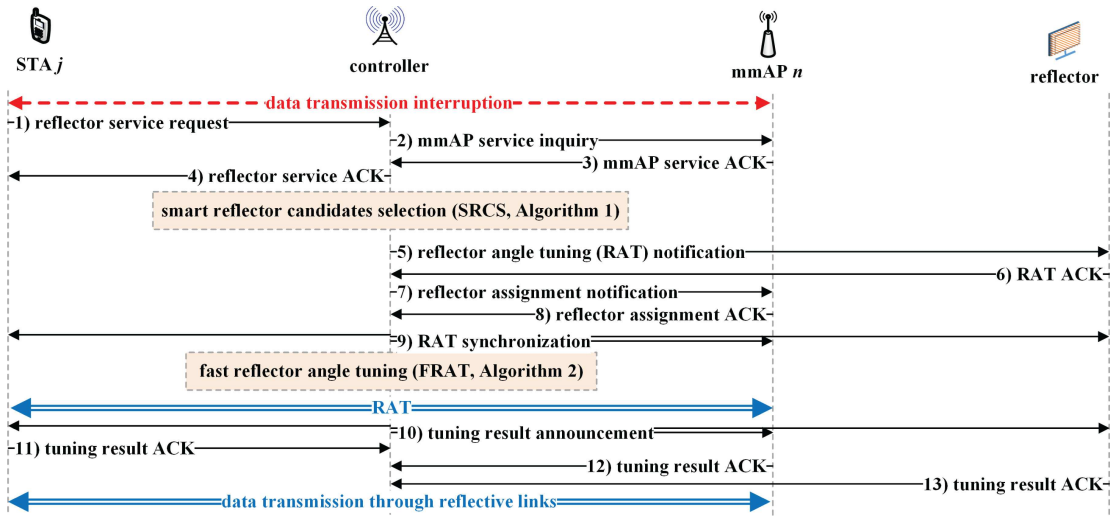

Fig. 3. The signaling process of reflective link establishment. The black solid lines and the blue double solid lines respectively represent the transmissions of control signals through reliable low-frequency bands and the transmissions of data signals through mmWave bands.

reflector candidates for RAT to further discover the final serving reflective links. However, there are several challenges for reflector candidate selection:

- The number of reflector candidates should be limited to reduce the cost and overhead introduced by more reflected beams.
- The channel state information (CSI) of a reflective link, i.e., the usability of a reflector, cannot be acquired before training its angle.
- The controller does not know exact locations of dynamic STAs and blockages, which can only be inferred from the previous interrupted transmissions.

To address these challenges, we propose a heuristic algorithm, namely SRCS, to target at a small group of reflectors with expected good performance. Denote the set of reflector candidates selected by SRCS algorithm for the interrupted transmission between mmAP n and STA i by RC_i^n. Given the previous transmission sector of mmAP n towards STA i by $S_i^n \in S^n$, where S^n is the sector set of mmAP n, the location of STA i and that of the blockages can be inferred inside or close to S_i^n. Since the reflectors surrounding mmAP n are recorded in *MTable* T_n and ordered based on their geometric locations classified by the sectors of mmAP n, as illustrated in Fig. 2, we first determine the geographical area to select RC_i^n in the form of mmAP sectors, and then find the specific RC_i^n located inside these sectors.

Since the locations of blockages are usually unpredictable, reflector candidates RC_i^n should be scattered over the environment. In this way, the unpredictable blockages are more likely to be circumvented due to the increased link diversity. Denote the size of RC_i^n, i.e., the number of selected reflector candidates, by $N_{i,RC}^n$, which is assigned by the controller. Since a reflector is only located inside one mmAP sector, denote the set of the corresponding sector area of each reflector in RC_i^n by SS_i^n, where each element sector $S_m^n \in SS_i^n$ represents the located sector of reflector m, and thus $|SS_i^n| = N_{i,RC}^n$. To realize high transmission diversity, reflector candidates in RC_i^n should be scattered to avoid clustering, and thus SS_i^n is first selected to restrict the locations of reflector candidates. Since the reflectors around the mmAP n and STA i pair are preferred, we only consider a half sectors surrounding S_i^n,

Algorithm 1: Smart Reflector Candidate Selection (SRCS).

Input: mmAP n (T_n, S^n, N_S^n), STA i (S_i^n, $N_{i,RC}^n$).
Output: selected reflector candidates RC_i^n.

// determining the targeted sector area SS_i^n

Initialization: $m = i - \left\lceil \frac{N_S^n}{4} \right\rceil$, count_{SS}=0;
if $N_{i,RC}^n < \left\lceil \frac{N_S^n}{2} \right\rceil$ **then**
  interv.SS$= \left\lfloor \left\lceil \frac{N_S^n}{2} \right\rceil / N_{i,RC}^n \right\rfloor$, $SS_i^n = \emptyset$;
  while $\text{count}_{SS} < N_{i,RC}^n$ **do**
    SS_i^n=$\{SS_i^n, S_m^n\}$, m=m+interv.SS, count_{SS}++;
  end while
else
  multi.SS$= \left\lfloor \left\lceil \frac{N_S^n}{2} \right\rceil / N_{i,RC}^n \right\rfloor$;
  SS_i^n=$\bigcup_{multi.SS} \{S_{i\pm m}^n | m \in [0, \left\lceil \frac{N_S^n}{2} \right\rceil]\}$;
  while $\text{count}_{SS} < N_{i,n}^{RC}$−multi.SS $\cdot \left\lceil \frac{N_S^n}{2} \right\rceil$ **do**
    SS_i^n=$\{SS_i^n, S_m^n\}$, m=m+interval.SS, count_{SS}++;
  end while
end if

// determining reflector candidates RC_i^n inside SS_i^n

Initialization: count_{RC}=0, $\text{RC}_i^n = \emptyset$;
while $\text{count}_{RC} < N_{i,RC}^n$ **do**
  Find the first element in the row corresponding to sector $SS_i^n(\text{count}_{\text{RC}})$ with idle state, and mark it as occupied;
  count_{RC}++;
end while

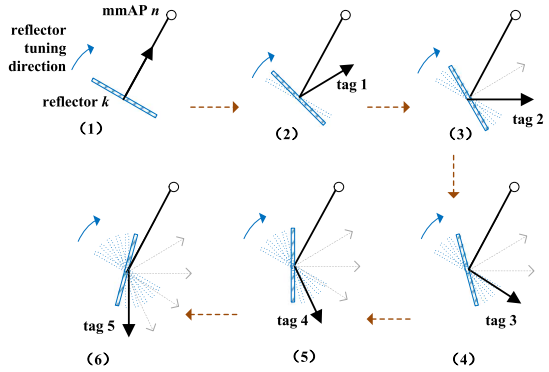

Fig. 4. The angle tuning process of tunable reflector design.

which is given as $\{S^n_{i\pm m} | m \in [0, \lceil N^n_S/4 \rceil]\}$ as the pool of SS^n_i selection, where N^n_S is the sector number of mmAP n. Note that the same sector may be selected more than once in SS^n_i when the required reflector candidates are more than the considered sectors, i.e., $N^n_{i,RC} > \lceil N^n_S/2 \rceil$. The basic idea of SS^n_i selection is their diversely scattered locations (Algorithm 1 line 1–13). When the number of assigned reflector candidates is small (say, $N^n_{i,RC} < \lceil N^n_S/2 \rceil$), the selected sectors of SS^n_i should try to be disconnected. Otherwise, the RC^n_i should be evenly distributed in the sector pool. Based on the determined SS^n_i, we select specific reflectors as RC^n_i inside each sector of SS^n_i. Since longer transmission distance may introduce higher attenuation and more blockages, we take the proximity benefits into account. Considering the unknown accurate location of STA i, the reflector closer to mmAP n is selected with priority. According to T_n defined in Section III-A, the reflectors inside any sector $S^n_i \in S^n$ are ordered based on their location to mmAP n as the ith row of T_n. Thus, the first reflector with availability state of *Idle* in the row (sector) belonging to SS^n_i is selected. To avoid duplicated assignment, the selected reflector should update its availability state as occupied in T_n. The detailed SRCS algorithm is summarized in Algorithm 1.

3) Fast Reflector Angle Tuning (FRAT): Different from the exhaustive search based beam alignment in IEEE 802.11ad standard, *mmRef* simplifies the operations of mmAPs by transmitting towards certain locations of reflector candidates, and the direction of a reflected beam is trained by tuning the angle of a reflector plate. As illustrated in Fig. 4, the angle of a reflector plate corresponds to the direction of the reflected beam, which is tagged in the training message based on the synchronization between an mmAP-reflector pair. Once a reflected beam can be used by the STA, i.e., the received signal strength satisfies the signal-to-noise-ratio (SNR) threshold ϵ_{SNR}, the ID of the reflector as well as its angle tag can be decoded by the STA from the RAT message and then sent to the controller. Thus, the reflector ID and the right tuning angle can be known. Note that when a reflector rotates 180°, the reflected beam sweeps through 360°. Define the unit of the tuned angle for each reflector by θ^R, and thus the times for the reflected beam sweeping the environment is $\lceil 180^\circ/\theta^R \rceil$. For mmAP n and STA i, denote the set of selected reflector and their corresponding angles by RI^n_i and RA^n_i, respectively. Our FRAT algorithm is designed to fast determine these two factors.

Algorithm 2: Fast Reflector Angle Tuning (FRAT).

Input: RC^n_i, $N^n_{i,R}$.
Output: RI^n_i, RA^n_i.
1: Initialization: Global variable $\text{count}_{RI} = N^n_{i,R}$, Local variable $\text{count}^k_{RA} = 0$;
Any reflector $k \in RC^n_i$ **does the following:**
// determining reflector tuning direction
2: **if** the sector number of reflector $k > i$ **then**
3: the tuning direction of k = *clockwise*;
4: **else**
5: the tuning direction of k = *counter-clockwise*
6: **end if**
// recording collaborative RAT transmission
7: **while** $\text{count}^k_{RA} < \lceil 180^\circ/\theta^R \rceil$ **do**
8: **if** $\text{count}_{RI} > 0$ **then**
9: **if** $\text{SNR}(\text{count}^k_{RA}) > \varepsilon_{\text{SNR}}$ **then**
10: Add reflector k and its angle ϕ to RI^n_i and RA^n_i;
11: $\text{count}_{RI} - -$;
12: **end if**
13: $\text{count}^k_{RA} + +$;
14: **end if**
15: **end while**

To unify the RAT process, each reflector is placed perpendicular to the mmAP as Fig. 4(1). A reflector plate rotates along either clockwise or counter-clockwise. To accelerate the RAT process, each reflector candidate first determines the proper tuning direction. According to the information of the previously interrupted transmission, STA i is quite possibly located inside or near the area of sector S^n_i. Since reflectors surrounding an mmAP are classified by their located sector area, the tuning direction can be selected based on these geographical information, where the reflected beam points towards sector S^n_i with priority. Assuming all sectors are clockwise sorted in the descending order, the reflector candidates located inside S^n_j with $j > i$ should tune along clockwise direction, otherwise along counter-clockwise direction (Algorithm 2 line 2–4). Based on the omni-directional reception, the STA sends the tag ϕ of the first available reflected beam to the controller. Since the physical RAT is time-consuming, all reflectors are tuning simultaneously to at most accelerate this process. Define the number of serving reflectors by $N^n_{i,R}$. The RAT process is terminated until the first $N^n_{i,R}$ reflectors are selected. The detailed process of FRAT algorithm is summarized in Algorithm 2.

The overhead of establishing a reflective link mainly comes from the RAT process, which is influenced by the location of the unpredictable blockages and STAs. In the worst case, a reflector needs to tune $\lceil 180^\circ/\theta^R \rceil$ times to sweep the 360° environment. To accelerate this process while providing high-quality reflective links, the two algorithms are proposed with low complexity $O(1)$. Specifically, SRCS first selects the most probably useful reflectors, i.e., the reflector candidates, around the mmAP-STA pair, and then FRAT determines the angle tuning directions.

Based on this, the reflectors are trained simultaneously until applicable reflective links are searched.

IV. Theoretical Performance Modeling

Although intuitively, *mmRef* can improve the system performance of mmWave WLANs, additional overhead like energy consumption and delay is also introduced. To quantify the expected performance benefits and evaluate the necessity of implementing *mmRef*, in this section, we theoretically analyze the system performance of the established reflective link transmissions based on stochastic geometry theory.

A. System model

We model the performance benefits by using the reflective links that are established under three cases, i.e., the proposed *mmRef*, the static reflector, and the environmental reflector. Specifically, under the static reflector case, small-piece metallic plates are deployed without the tunable function, where the available reflectors might be largely reduced due to the reflection requirement; under the environmental reflector case, we do not change the transmission environment, where reflective links are established through bouncing off the environmental reflectors with poor reflectance, such as the wood or concrete wall. In the following, we define *mmRef*, the static reflector, and the environmental reflector as Case 1-3, respectively, for simplicity.

Considering the overall transmission environment augmentation, tunable reflectors should be specifically deployed in places of interest according to specific WLAN environments. Due to the difficulty of characterizing the specialized reflector placement, this work assumes randomly placed reflectors for tractable analytical results. Given the fact that the strategic reflector placement outperforms the random placement, our analytical results based on randomly distributed reflectors can be considered as the worst case, which quantifies the lower bounds of performance benefits. Specifically, the distributions of reflectors in Case 1 and 2 are modeled as Poisson Point Process (PPP) Φ_1 and Φ_2, respectively. For a fair comparison, the same reflector intensity are assumed in Case 1 and 2 denoted by λ_1. However, without the tunable function, the strict reflection requirement restricts the number of available reflectors in Case 2, where only a proportional reflectors can serve a certain STA. According to the thinning theory of PPP [25], [26], the distribution of available reflectors in Case 2 can be modeled as PPP Φ_2 with intensity $\lambda_2 = \rho\lambda_1$, where $\rho \in [0, 1]$ is the available reflector proportion of the total deployed reflectors. The locations of environmental reflectors in Case 3 are also modeled as PPP Φ_3 with intensity λ_3. For the sake of convenience, the environmental reflectors of Case 3 are assumed to exhibit identical reflectance, which matches the fact of surrounding environments with wood or concrete walls. Note taht the relationship between λ_1 and λ_3 is determined by the system settings, such as the intensity of deployed reflectors, the reflectance of transmission environment, etc.

To model the channel condition, independent Nakagami fading with parameter N_h is assumed [24], [27], [28], where the fading power is $h \sim \Gamma(N_h, 1/N_h)$. The standard path-loss function, $L_j(d) = C_j d^{-\alpha_j}$, is applied based on channel condition $j \in \{\mathrm{LOS}, \mathrm{NLOS}\}$, where d is the transmission distance; C_j and α_j are respectively the path-loss intercept and exponent. The blocking conditions, i.e., LOS or non-LOS (NLOS) link, are modeled based on the random shape blockage model [5], [24], [27], [28], where the LOS and NLOS probability are respectively given by

$$A_{\mathrm{LOS}} = \Pr(j = \mathrm{LOS}) = \mathrm{e}^{-\beta d}, \tag{1}$$

and

$$A_{\mathrm{NLOS}} = \Pr(j = NLOS) = 1 - \mathrm{e}^{-\beta d}, \tag{2}$$

where d is the link distance and β is a constant parameter determined by the intensity and average size of the blockages. Note that the definitions of LOS and NLOS probabilities correspond to the fact that the longer transmission distance, the higher probability of blocking. The received signal strength in Case $i \in \{1, 2, 3\}$ can be given by $P_{r,i} = P_t G_0 \gamma_i h L(d)$, where P_t is the transmit power of an mmAP; G_0 is the aligned directional antenna gain of an mmAP-STA pair; γ_i is the reflectance of the reflectors in Case i. Since the reflected beam with the strongest signal strength is preferred, based on our received beam strength $P_{r,i}$, the shortest reflective link should be selected in all three cases. Most existing work using stochastic geometry theory, characterizes the system performance based on the geographically nearest device, where the probability distribution function (PDF) of distance to the nearest PPP distributed device is involved [5], [24], [27], [28]. Instead of only considering the distance d_1 between an mmAP and the nearest PPP distributed reflectors, the distance of a reflective link, D, additionally involves the distance between an STA and that reflector, d_2, as illustrated in Fig. 3. According to the displacement theorem of PPP [25], [26], we map the point process of the mirrored mmAPs to the corresponding point process of reflectors. Without loss of accuracy, we assume the STA and mmAP are respectively located at (0,0) and $(D_0, 0)$. We derive the cumulative distribution function (CDF) of the shortest reflective link distance D in Lemma 1.

Lemma 1: The CDF of the distance of the shortest reflective link D_{min} is given by

$$\Pr(D_{\min} > d) = \exp\left\{-\frac{\lambda d\sqrt{d^2 - D_0^2}}{4} \times \left[\arctan\left(\sqrt{\frac{d - D_0}{d + D_0}}\right) + \arctan\left(\sqrt{\frac{d + D_0}{d - D_0}}\right)\right]\right\}, \tag{3}$$

where λ is the intensity of reflectors and D_0 is the distance between an STA and an mmAP.

Proof: As shown in Fig. 5, the distance of a reflective link from Tx to Rx is equal to the direct distance from that Tx to the mirrored Rx. Thus we turn to analyze the latter distance. According to the displacement theory [25], [26], the locations of the mirrored Rxs can be matched to that of PPP distributed reflectors, where the point process of the mirrored Rxs is still PPP. Without loss of generality, Tx is located at the origin. The CDF of the shortest reflective link distance of Tx, i.e. the distance

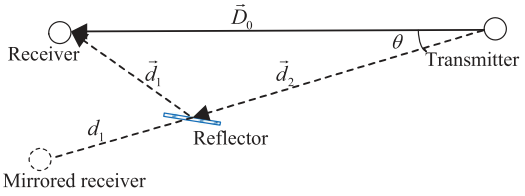

Fig. 5. Modeling the mmWave transmission through a reflective link.

from Tx to the nearest mirrored Rx is given by

$$\Pr\{D_{min} > d\} = \mathrm{e}^{-\Lambda'(B(o,d))} = \mathrm{e}^{-\lambda \int_{R^2} p(x,B(o,d))\mathrm{d}x},$$

where $B(o,d)$ is the circle region with radius d centered at the origin and $p(x,B(o,d))$ is the probability that there is no mirrored Rx inside the circle with radius x, i.e., there is no reflector inside $B(o,d)$. To further analyze the above integral term, the polar coordination is introduced to assist the derivation, and thus the above integral term can be given by

$$\begin{aligned}
&\int_{R^2} p\left(x, B(o,d)\right)\mathrm{d}x \\
&= \int_{R^2} p\left(d_1+d_2, B(o,d)\right)\mathrm{d}d_1\mathrm{d}d_2 \\
&\overset{(a)}{=} \int_0^{\infty}\int_0^{2\pi} d_2 p\left(d_2+\sqrt{d_2^2+D_0^2-2d_2D_0\cos\theta}, B(o,d)\right) \\
&\quad \times \mathrm{d}\theta\mathrm{d}d_2 \\
&\overset{(b)}{=} \int_0^{\infty}\int_{|D_0-d_2|}^{D_0+d_2} \frac{2d_2d_1\cdot p\left(d_1+d_2, B(o,d)\right)}{\sqrt{\left((D_0+d_2)^2-d_1^2\right)\left(d_1^2-(D_0-d_2)^2\right)}} \\
&\quad \times \mathrm{d}d_1\mathrm{d}d_2,
\end{aligned}$$

where in (a) θ is the angle between $\vec{D}_0$ and $\vec{d}_2$. Note $\vec{D}_0$ and $\vec{d}_2$ are respectively the vectors from Tx to Rx and from Tx to the reflector with corresponding distance D and d_2. (b) comes from the cosine theorem, and thus we have

$$\mathrm{d}\theta = \frac{\mathrm{d}\theta}{\mathrm{d}d_1}\mathrm{d}d_1 = \frac{2d_1\cdot\mathrm{d}d_1}{\sqrt{\left((D_0+d_2)^2-d_1^2\right)\left(d_1^2-(D_0-d_2)^2\right)}}.$$

Given that $x \geq d_1+d_2$ when $p(x,B(o,d))=1$, d_1 and d_2 should satisfy the following constraints:

$$\begin{cases} d_1+d_2 > D_0 \\ d_1+D_0 > d_2 \\ D_0+d_2 > d_1 \\ d_1+d_2 < d \end{cases}$$

otherwise $p(x,B(o,d))=0$. Thus, we have

$$\begin{aligned}
&\int_{R^2} p\left(x,B(o,d)\right)\mathrm{d}r_1\mathrm{d}r_2 \\
&= \int_0^{\frac{d-D_0}{2}}\int_{(D_0-d_2)^2}^{(D_0+d_2)^2} \frac{d_2}{\sqrt{\left((D_0+d_2)^2-t\right)\left(t-(D_0-d_2)^2\right)}} \\
&\quad \times \mathrm{d}t\mathrm{d}d_2 \\
&\quad + \int_{\frac{d-D_0}{2}}^{\frac{d+D_0}{2}}\int_{(D_0-d_2)^2}^{(d-d_2)^2} \frac{d_2}{\sqrt{\left((D_0+d_2)^2-t\right)\left(t-(D_0-d_2)^2\right)}} \\
&\quad \times \mathrm{d}t\mathrm{d}d_2 \\
&\overset{(a)}{=} \frac{\pi D_0^2}{8}+\frac{\pi d^2}{8}+\int_{\frac{d-D_0}{2}}^{\frac{d+D_0}{2}} d_2\arcsin\left(\frac{d^2-D_0^2}{2D_0d_2}-\frac{d}{D_0}\right)\mathrm{d}d_2.
\end{aligned}$$

The integral term of (a) can be further calculated as

$$\begin{aligned}
&\int_{\frac{d-D_0}{2}}^{\frac{d+D_0}{2}} r_2\arcsin\left(\frac{d^2-D^2}{2D_0r_2}-\frac{d}{D_0}\right)\mathrm{d}r_2 = -\frac{\pi\left(d^2+D_0^2\right)}{8} \\
&-\frac{d\sqrt{d^2-D_0^2}}{4}\left\{\arctan\left(-\sqrt{\frac{d-D_0}{d+D_0}}\right)-\arctan\left(\sqrt{\frac{d+D_0}{d-D_0}}\right)\right\},
\end{aligned}$$

and thus we derive the final CDF in Lemma 1. ■

B. Outage Probability

Unlike conventional transmissions through sub-6 GHz bands, transmissions with narrow directional beams as well as the vulnerability of blockages through mmWave bands inherently generate less interference [5], especially with limited number of simultaneous beams in 802.11ad systems. To simplify our model, we focus on the signal-to-noise-ratio (SNR) while ignoring the interference, which can be supported by interference mitigation technologies [7]. The SNR of the transmission through a reflective link in Case $i \in \{1,2,3\}$ can be given by

$$\mathrm{SNR}_{\mathrm{r,i}} = \frac{P_tG_0\gamma_ihL(D)}{\sigma^2}, \tag{4}$$

where σ^2 is the power of additive Gaussian noise. Note that the SNR of transmissions through the direct link can be expressed by (5) with $\gamma_i=1$ and $D=D_0$. The outage occurs when the SNR is lower than the threshold ε, and thus the outage probability of the mmWave transmission through a reflective link is given in Theorem 1.

Theorem 1: The outage probability of the mmWave transmission through a reflective link in Case $i \in \{1,2,3\}$ can be given by

$$\begin{aligned}
\Pr{}^{i}_{O,r} \triangleq &\sum_{n=0}^{N_h}\binom{N_h}{n}(-1)^n \\
&\times\left\{G_i+\int_{D_0}^{\infty}\Pr\left(D>d\right)g'_i(d)\mathrm{d}d\right\},
\end{aligned} \tag{5}$$

where $G_i = e^{-\beta D_0-\frac{b_iD_0^{\alpha_L}}{C_L}}+(1-e^{-\beta D_0})e^{-\frac{b_iD_0^{\alpha_N}}{C_N}}$ and $b_i = N_h(N_h!)^{-1/N_h}\varepsilon\sigma^2/(P_tG_0\gamma_i)$. $\Pr(D>d)$ is given in (3), and

$$\begin{aligned}
g'_i(d) = &-\left(\beta+\frac{b_i\alpha_Ld^{\alpha_L-1}}{C_L}\right)e^{-\beta d-\frac{b_id^{\alpha_L}}{C_L}} \\
&-\left(\frac{b_i\alpha_Nd^{\alpha_N-1}}{C_N}-\left(\frac{b_i\alpha_Nd^{\alpha_N-1}}{C_N}+\beta\right)e^{-\beta d}\right)e^{-\frac{b_id^{\alpha_N}}{C_N}}.
\end{aligned}$$

Proof: According to the definition of outage probability, we derive its general expression for Case $i \in \{1,2,3\}$,

$$\begin{aligned}\Pr_{O,r}^{i} &= \sum_{j\in\{\mathrm{LOS},\mathrm{NLOS}\}} \Pr(j)\Pr\left(\mathrm{SNR}_{r,i} < \varepsilon | j\right) \\ &= \sum_{j\in\{\mathrm{LOS},\mathrm{NLOS}\}} \Pr(j)\Pr\left(h < \tfrac{\varepsilon\sigma^2}{P_t G_0 \gamma C_j D^{-\alpha_j}}\right) \\ &\overset{(a)}{\approx} \int_{D_0}^{\infty} \sum_{j\in\{\mathrm{LOS},\mathrm{NLOS}\}} \Pr(j) \sum_{n=0}^{N_h} \binom{N_h}{n} (-1)^n \\ &\quad \times \exp\left(\tfrac{-N_h(N_h!)^{-1/N_h}\varepsilon\sigma^2 n}{P_t G_0 \gamma_i C_j d^{-\alpha_j}}\right) f_D(d)\mathrm{d}d \\ &= \sum_{n=0}^{N_h} \binom{N_h}{n} (-1)^n \int_{D_0}^{\infty} g_i(d) f_D(d)\mathrm{d}d,\end{aligned}$$

where $g_i(x) = e^{-\beta d - b_i d^{\alpha_L}/C_L} + (1-e^{-\beta d})e^{-b_i d^{\alpha_N}/C_N}$ and $b_i = N_h(N_h!)^{-1/N_h}\varepsilon\sigma^2/(P_t G_0 \gamma_i)$. In (a), according to Theorem 1 of [29], the normalized gamma random variable h is tightly bounded by

$$P\left(h < \gamma\right) \geq \left[1 - e^{-\eta\gamma}\right]^{N_h} = \sum_{n=0}^{N_h} \binom{N_h}{n} (-1)^n e^{-\eta\gamma n},$$

where $\eta = N_h(N_h!)^{-1/N_h}$. With some mathematical manipulations, we complete our proof. ■

As aforementioned, *mmRef* aims at fast recovering interrupted transmissions, where a reflective link can be regarded as a backup link to lower the outage probability. Only when these two links simultaneously become outage, can the outage occur for an STA. Assume that the outages of the two links are independent, which is valid for most situations with small sized blockages in the middle of transmissions. Based on the outage probability derived in Theorem 1, we obtain the outage probability when the mmWave transmission of an STA is assisted by one reflective link, which is given by $\Pr_O^i = \Pr_{O,d} \cdot \Pr_{O,r}^i$ for Case $i \in \{1,2,3\}$. Note that $\Pr_{O,d}$ is the outage probability of a direct link, which can be a special case of outage probability in Theorem 1 with $\gamma_i = 1$ and $D = D_0$. According to the expression of $\Pr_O^i$, we can infer that the outage for an STA can be further reduced when multiple reflective links are prepared for serving this STA.

C. Transmission Throughput

Assuming adaptive modulation and coding are used, we define the expected link throughput $\mathcal{C}$ from Shannon's theorem, that is, $\mathcal{C} = \mathrm{E}[B\ln(1+\mathrm{SNR})]$, where B is the transmission bandwidth of a link. According to the SNR in (4) and the reflective link distance distribution in (3), we derive the expected throughput of the transmission through a reflective link in *Theorem 2*.

Theorem 2: The expected throughput of the transmission through a reflective link in Case $i \in \{1,2,3\}$ is given in (6) at the bottom of this page, where $b_i = \frac{N_h(N_h!)^{-1/N_h}\sigma^2}{P_t G_0 \gamma_i}$ and $\mathrm{E}_1(a)$ is the exponential integral, i.e., $\mathrm{E}_1(a) = \int_a^{\infty} e^{-u}/u\mathrm{d}u$.

Proof: According to the definition of throughput $\mathcal{C}$, we have

$$\begin{aligned}\mathcal{C}_{r,i}/B &= \mathbb{E}\left[\ln\left(1+\mathrm{SNR}_{r,i}\right)\right] \\ &= \int_{D_0}^{\infty} f_D(d) \int_0^{\infty} \Pr\left(h > \frac{(e^t-1)\,\sigma^2}{P_t G_0 \gamma_i C_i d^{-\alpha_i}}\right)\mathrm{d}t\mathrm{d}d \\ &\overset{(a)}{=} \sum_{n=1}^{N_h} (-1)^{n+1}\binom{N_h}{n} \int_{D_0}^{\infty} f_D(d) \int_0^{\infty} \Bigg[e^{-\beta d - \frac{b_i n(e^t-1)}{C_L d^{-\alpha_L}}} \\ &\quad + \left(1-e^{-\beta d}\right) e^{-\frac{b_i n(e^t-1)}{C_N d^{-\alpha_N}}} \Bigg]\mathrm{d}t\mathrm{d}d \\ &\overset{(b)}{=} \sum_{n=1}^{N_h} \frac{(-1)^{n+1}\binom{N_h}{n}}{b_i n} \\ &\quad \times \Bigg\{ C_L \int_{D_0}^{\infty} f_D(d) d^{-\alpha_L} e^{\frac{b_i n}{C_L d^{-\alpha_L}} - \beta d} \mathrm{E}_1\left(\frac{b_i n}{C_L d^{-\alpha_L}}\right)\mathrm{d}d \\ &\quad + C_N \int_{D_0}^{\infty} f_D(d)\left(1-e^{-\beta d}\right) d^{-\alpha_N} e^{\frac{b_i n}{C_N d^{-\alpha_N}}} \mathrm{E}_1\left(\frac{b_i n}{C_N d^{-\alpha_N}}\right)\mathrm{d}d \Bigg\},\end{aligned}$$

where (a) comes from the step (a) in Appendix 2. From the integral expression in (b), we finally derive (6) with some mathematical manipulations. ■

According to *Theorem 2*, when the transmission distance D is equal to D_0, and the reflectance $\gamma = 1$, we can derive transmission throughput of a direct link, which is given below.

$$\begin{aligned}\mathcal{C}_{r,i} \triangleq B \sum_{n=1}^{N_h} \frac{(-1)^{n+1}\binom{N_h}{n}}{b_i n} \times \Bigg[& C_L D_0^{-\alpha_L} e^{\frac{b_i n}{C_L D_0^{-\alpha_L}} - \beta D_0} \mathrm{E}_1\left(\frac{b_i n}{C_L D_0^{-\alpha_L}}\right) \\ & + C_N\left(1-e^{-\beta D_0}\right) D_0^{-\alpha_N} e^{\frac{b_i n}{C_N D_0^{-\alpha_N}}} \mathrm{E}_1\left(\frac{b_i n}{C_N D_0^{-\alpha_N}}\right) \\ & + C_L \int_{D_0}^{\infty} \Pr\left(D > d\right)\left(-\alpha_L d^{-\alpha_L - 1} e^{-\beta d} + \mathrm{E}_1\left(\frac{b_i n}{C_L d^{-\alpha_L}}\right) d^{-\alpha_L - 1}\left(\frac{\alpha_L b_i n}{C_L} d^{\alpha_L} - \beta d - \alpha_L\right) e^{\frac{b_i n}{C_L} d^{\alpha_L} - \beta d}\right)\mathrm{d}d \\ & + C_N \int_{D_0}^{\infty} \Pr\left(D > d\right)\left(-\alpha_N d^{-\alpha_N - 1}\left(1-e^{-\beta d}\right)\right. \\ & \left. + \mathrm{E}_1\left(\frac{b_i n}{C_N d^{-\alpha_N}}\right) d^{-\alpha_N - 1}\left(\left(\frac{\alpha_N b_i n}{C_N} d^{\alpha_N} - \alpha_L\right) e^{\beta d} - \frac{\alpha_N b_i n}{C_N} d^{\alpha_N} + \beta d + \alpha_L\right) e^{\frac{b_i n}{C_L} d^{\alpha_L} - \beta d}\right)\mathrm{d}d \Bigg]\end{aligned} \tag{6}$$

TABLE I
PARAMETERS OF PERFORMANCE EVALUATION

Parameter	Value	Description
D_0	10 m	direct link distance
α_L, α_N	2, 4	pathloss exponent (LOS, NLOS)
N_h	3	Nakagami fading parameter
β	0.008	parameter of blockage model
λ_1	$0.03/m^2$	intensity of reflectors in *mmRef*
γ_1,γ_2,γ_3	1, 1, 0.5	reflector reflectance (case 1, 2, 3)
P_s/σ^2	5×10^5	transmit power to noise power ratio
ϵ	0 dB	SNR threshold

Corollary 1: The expected direct link throughput in an mmWave transmission with distance D_0 can be given by

$$\mathcal{C}_d \triangleq B\sum_{n=1}^{N_h}(-1)^{n+1}\binom{N_h}{n}\times\left[e^{\frac{bD_0^{\alpha_L}n}{C_L}-\beta D_0}\mathrm{E}_1\left(\frac{bD_0^{\alpha_L}n}{C_L}\right)+\left(1-e^{-\beta D_0}\right)e^{\frac{bD_0^{\alpha_N}n}{C_N}}\mathrm{E}_1\left(\frac{bD_0^{\alpha_N}n}{C_N}\right)\right],$$

where $b=\frac{N_h(N_h!)^{-1/N_h}\sigma^2}{P_tG_0}$ and $\mathrm{E}_1(a)$ is the exponential integral.

During a beacon interval of WLAN transmissions, given the duration of the transmission through the direct link by t_d and that through a reflective link by $t_{r,i}$, the traffic amount of an mmAP-STA pair in Case $i\in\{1,2,3\}$ can be given by

$$T_i=\mathcal{C}_d t_d+\mathcal{C}_{r,i}t_{r,i},\quad i\in\{1,2,3\}, \tag{7}$$

where the t_d and $t_{r,i}$ are influenced by the specific situation of that mmAP-STA pair, such as the payload, the channel condition, the overhead of reflective link establishment, etc.

V. PERFORMANCE EVALUATION

As a proof of concept, this work focuses on how to implement *mmRef* and what performance benefits that can be expected from the established reflective links. Based on analysis from the previous two sections, simulation and numerical results are presented. To verify the effectiveness of implementing *mmRef* to establish reflective links, we first evaluate the performance of SRCS and FRAT algorithms. Then, based on the theoretical modeling, we evaluate the outage performance followed by the transmission throughput to examine the performance benefits expected from *mmRef*. Unless specified otherwise, the system parameters in Table I will be used [5], [24], [27], [28].

A. Reflective-Link Establishment Performance

Since the reflective link establishment scheme is crucial to determine the quality of *mmRef* services, the performance of establishing reflective links, i.e., SRCS and FRAT algorithms, are evaluated. We consider a 40 m × 40 m WLAN environment with reflector intensity 0.1/m^2, and the distance between a pair of mmAP and STA is 10 meters. To evaluate the performance of SRCS algorithm, we examine the quality of the reflective links established by using the reflector candidates selected by SRCS algorithm under different blockage conditions, i.e., different blockage sizes and blockage locations. In Fig. 6(a), the frequency of the successful recovery (LOS transmission) is a function of the blockage location between the mmAP and the STA, under different blockage sizes. Note that a large blockage located close to the end device, i.e., the mmAP or the STA, is usually hard to be circumvented. We observe that SRCS algorithm can successfully recover the interrupted transmissions, even when a 6-meter long blockage is 0.5 meters away from the end device. Meanwhile, under various blockage conditions, SRCS algorithm significantly outperforms the random reflector selection scheme. In addition, to evaluate the performance of FRAT algorithm, we examine the average tuning times used to adjust the reflectors at appropriate angles as a function of the number of the required serving reflectors in Fig. 6(b), where the tuned reflectors are reflector candidates selected by SRCS algorithm. Note that the larger angle tuning times mean the longer training time, and the angle tuning granularity is 2° in our evaluation. We observe that the FRAT algorithm significantly reduces the overhead of RAT process compared with random angle tuning strategy, especially when more serving reflectors are required (i.e., a larger $N_{i,R}^n$). Besides, FRAT algorithm performs better when more reflector candidates is involved in RAT process (i.e., a larger $N_{i,RC}^n$), where the serving reflectors with appropriately tuned angles can be quickly found.

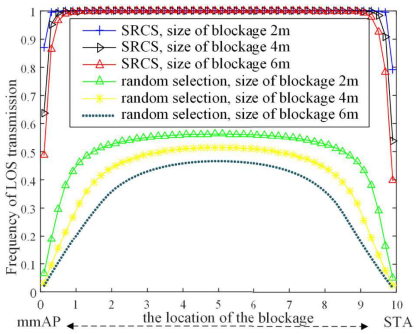

(a)

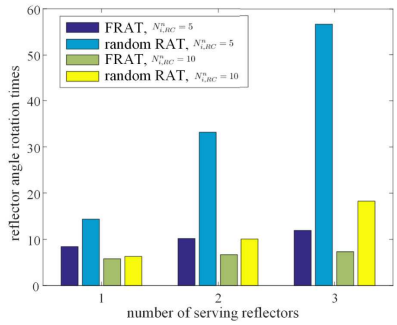

(b)

Fig. 6. Performance of reflective link establishment schemes. (a) SRCS algorithm. (b) FRAT algorithm.

B. MmRef Service Performance

Based on the analytical results in Section IV, we evaluate the performance benefits expected from *mmRef* services. For a fair comparison, the same system settings are utilized for the

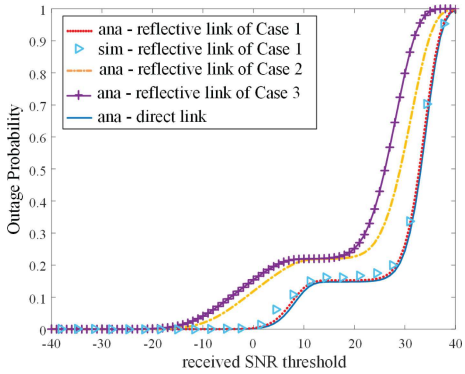

Fig. 7. The overall outage performance comparison.

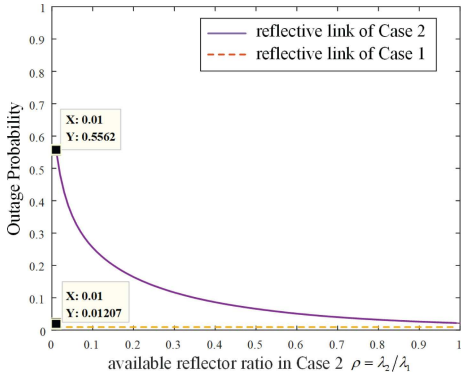

Fig. 8. The outage performance comparison between Case 1 and 2.

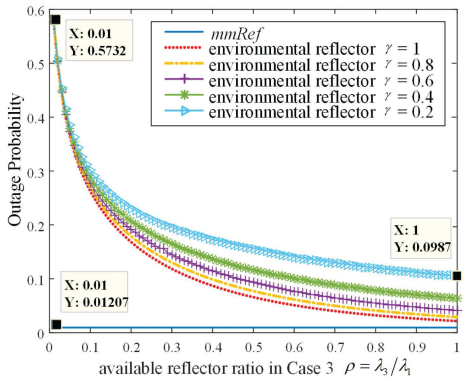

Fig. 9. The outage performance comparison between Case 1 and 3.

three mmWave WLAN transmission Cases, i.e., *mmRef*, static deployed reflectors and normal WLAN environment (detailed in Section IV-A). The comparison of outage performance is first evaluated to examine the quality of transmission through the reflective link. Then the system throughput is investigated providing further insights for *mmRef* implementation. To validate the accuracy of our analytical results, Monte Carlo simulation results are provided with the same parameters through 10,000 independent realizations in a square area of 500 m $\times$ 500 m.

Fig. 7–9 illustrates the outage performance comparison among the three cases. The overall performance of the three cases are evaluated in Fig. 7. The outage probability is a function

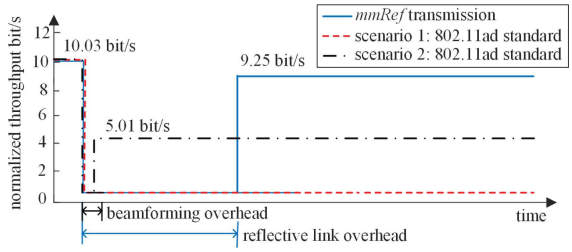

Fig. 10. The comparison of normalized transmission throughput.

of the received SNR threshold, where $\lambda_2 = \lambda_3 = 0.003/\text{m}^2$ and $\gamma_3 = 0.5$. we observe the outage probability of Case 1 is much lower than that of Case 2 and 3, which validates the effectiveness of the reflective link provided by *mmRef*. In addition, the outage probability of the reflective link from *mmRef* is close to that of the direct link, which reveals that although outages occur more frequently in reflective links due to their longer distances, the performance of *mmRef* is very close to the best. To quantify the performance enhancement by *mmRef* system, given the same number of the deployed reflectors in Case 1 and 2, Fig. 8 compares the outage probabilities of Case 1 and 2 as a function of the ratio of available reflectors in Case 2, i.e., $\rho_{1,2} = \lambda_2/\lambda_1$. Note that the fixed angle of a reflector plate in Case 2 limits its serving area, and thus only part of reflectors are available to serve an mmAP and STA pair. We observe that when $\rho_{1,2} = 0.01$, the outage probability of case 2 can be nearly 30 times higher compared with that of *mmRef*. This reveals that much more static reflectors are needed for in Case 2 to achieve the same performance. Similar comparison between Case 1 and 3 is illustrated in Fig. 9, where the outage probability is a function of the ratio of available environmental reflectors in Case 3. Different from Case 2, the environmental reflectors in Case 3 may largely absorb the signal power with very low reflectance γ_3. We observe that the outage becomes severe when γ_3 becomes small. Even with enough environmental reflectors, i.e., $\rho_{1,3} = 1$, the outage probability of Case 3 is still 5 times higher than that of *mmRef*. Moreover, the poor reflection characteristic due to the property of different materials, such as wood and concrete [13], [22], cannot be overcome. Therefore, compared with Case 2 and 3, robust mmWave transmissions through reflective links can be expected by implementing *mmRef*. Simulation results further validate the accuracy of our modeling. Although the outage probability of the analytical results are a little lower than that of the simulation results, the analytical results can be a lower bound effectively characterizing the outage performance of mmWave transmissions through reflective links.

The throughput comparison among *mmRef* and 802.11ad systems is illustrated as a function of time in Fig. 10, where the bandwidth is assumed to be normalized. By using the default system parameters in Table I, the normalized throughput values are calculated based on the numerical results in Section IV-C. In our simulation, an interruption occurs at an early stage of transmission with 10.03 bit/s. For *mmRef* system, the reflective link establishment is immediately activated, and the throughput of the recovered transmission through a reflective link can be 9.25 bit/s, which is as good as the previous throughput value.

Due to the difficulty to quantify the overhead of establishing a reflective link, an estimated delay is qualitatively used. For 802.11ad system, a re-training process is also immediately activated through exhaustive beam sweeping. However, due to the limited number of available environmental reflectors as well as their poor reflectance, the recovery performance would be largely degraded. Two environmental reflector scenarios are used in our simulation for comparison. In the first scenario with environmental reflector intensity $\lambda_3 = 10^6/m^2$, even the strongest reflected signal cannot satisfy the required SNR threshold, defined as 0 dB. In the second reflection-friendly scenario with $\lambda_3 = 10^3/m^2$, the recovered throughput is only half of the previous value.

We observe that when the remaining transmission time is large, the *mmRef* transmission is a better choice, where the sacrificed reflective link overhead is worthwhile for a larger recovered throughput. In addition, without specially deploying reflectors, the available reflectors with the right angle in the environment is usually rare, such as in scenario 1, and thus the interrupted transmission can be hardly recovered by 802.11ad systems. Therefore, considering the unpredictability of environmental reflection based on the 802.11ad standard, the *mmRef* service is imperative for robust mmWave WLAN transmissions with significant throughput improvement. Besides, the reduced outages by the *mmRef* system can conserve the energy and spectrum expenditures for both the operator and STAs.

VI. Conclusion

In this paper, we have focused on mmWave WLANs as an exemplary scenario, and investigated how to augment the transmission environments to boost the network performance while not damaging the aesthetic nature of the environment. By deploying tunable reflectors, the highly-reflective cheap metallic plates with adjustable angles, we have proposed a novel adaptive mechanism for transmission environment reconfiguration, called *mmRef*, which effectively tunes the angels of the deployed reflectors when necessary. Specifically, we have developed the system architecture from the idea of decoupling control-/data-signaling. Meanwhile, based on the centralized control, a reflective link establishment scheme is designed including the signaling process based on SRCS and FRAT algorithms. To evaluate the expected benefits, the outage probability and the transmission throughput through reflective link transmissions are theoretically evaluated by using the stochastic geometry theory. Simulation and numerical results have demonstrated the effectiveness of the *mmRef* mechanism and the significant performance gain from our design. We expect our preliminary study will inspire more thorough research on this line.

References

[1] L. Zhang, L. Yan, B. Lin, Y. Fang, and X. Fang, "Tunable reflectors enabled environment augmentation for better mmWave WLANs," in *Proc. IEEE/CIC Int. Conf. Commun. China*, Aug. 11-13. 2019, pp. 7–12.

[2] V. Garg, *Wireless Communications & Networking*. Amsterdam, The Netherlands: Elsevier, 2010.

[3] J. Liu, N. Kato, J. Ma, and N. Kadowaki, "Device-to-device communication in LTE-advanced networks: A survey," *IEEE Commun. Surveys Tut.*, vol. 17, no. 4, pp. 1923–1940, Oct.–Dec. 2015.

[4] Y. Niu, Y. Li, D. Jin, L. Su, and A. V. Vasilakos, "A survey of millimeter wave communications (mmwave) for 5G: Opportunities and challenges," *Wireless Netw.*, vol. 21, no. 8, pp. 2657–2676, 2015.

[5] J. G. Andrews, T. Bai, M. N. Kulkarni, A. Alkhateeb, A. K. Gupta, and R. W. Heath, "Modeling and analyzing millimeter wave cellular systems," *IEEE Trans. Commun.*, vol. 65, no. 1, pp. 403–430, Jan. 2017.

[6] A. Ghosh *et al.*, "Millimeter-wave enhanced local area systems: A high-data-rate approach for future wireless networks," *IEEE J. Sel. Areas Commun.*, vol. 32, no. 6, pp. 1152–1163, Jun. 2014.

[7] P. Zhou *et al.*, "Ieee 802.11 ay-based mmwave wlans: Design challenges and solutions," *IEEE Commun. Surveys Tut.*, vol. 20, no. 3, pp. 1654–1681, Jul.–Sep. 2018.

[8] H. Shokri-Ghadikolaei, C. Fischione, P. Popovski, and M. Zorzi, "Design aspects of short-range millimeter-wave networks: A mac layer perspective," *IEEE Netw.*, vol. 30, no. 3, pp. 88–96, Jun. 2016.

[9] Q. Xue, X. Fang, and C.-X. Wang, "Beamspace su-mimo for future millimeter wave wireless communications," *IEEE J. Sel. Areas Commun.*, vol. 35, no. 7, pp. 1564–1575, Jul. 2017.

[10] X. Zhou *et al.*, "Mirror mirror on the ceiling: Flexible wireless links for data centers," *ACM SIGCOMM Comput. Commun. Rev.*, vol. 42, no. 4, pp. 443–454, 2012.

[11] Z. Shi, R. Lu, J. Chen, and X. S. Shen, "Three-dimensional spatial multiplexing for directional millimeter-wave communications in multi-cubicle office environments," in *Proc. IEEE Global Commun. Conf. (GLOBECOM)*, 2013, pp. 4384–4389.

[12] Z. Genc, U. H. Rizvi, E. Onur, and I. Niemegeers, "Robust 60 ghz indoor connectivity: Is it possible with reflections?" in *Proc. IEEE 71st Veh. Technol. Conf.*, 2010, pp. 1–5.

[13] T. S. Rappaport *et al.*, "Millimeter wave mobile communications for 5G cellular: It will work!" *IEEE Access*, vol. 1, pp. 335–349, 2013.

[14] L. Zhang, X. Chen, Y. Fang, X. Huang, and X. Fang, "Learning-based mmwave V2I environment augmentation through tunable reflectors," in *Proc. IEEE Global Commun. Conf. (GLOBECOM)*, Waikoloa, HI, USA, Dec. 9-13 2019, pp. 1–6.

[15] X. Tan, Z. Sun, D. Koutsonikolas, and J. M. Jornet, "Enabling indoor mobile millimeter-wave networks based on smart reflect-arrays," in *Proc. IEEE INFOCOM Conf. Comput. Commun.*, 2018, pp. 270–278.

[16] M. Di Renzo *et al.*, "Smart radio environments empowered by reconfigurable AI meta-surfaces: An idea whose time has come," *EURASIP J. Wireless Commun. Netw.*, vol. 2019, no. 1, pp. 1–20, 2019.

[17] L. Yan, X. Fang, and Y. Fang, "Control and data signaling decoupled architecture for railway wireless networks," *IEEE Wireless Commun.*, vol. 22, no. 1, pp. 103–111, Feb. 2015.

[18] O. Semiari, W. Saad, M. Bennis, and M. Debbah, "Integrated millimeter wave and sub-6 Ghz wireless networks: A roadmap for joint mobile broadband and ultra-reliable low-latency communications," *IEEE Wireless Commun.*, vol. 26, no. 2, pp. 109–115, Apr. 2019.

[19] S. Hiranandani, S. Mohadikar, W. Khawaja, O. Ozdemir, I. Guvenc, and D. Matolak, "Effect of passive reflectors on the coverage of ieee 802.11 ad mmwave systems," in *Proc. IEEE 88th Veh. Technol. Conf. (VTC-Fall)*, 2018, pp. 1–6.

[20] T. Nitsche, C. Cordeiro, A. B Flores, E. W. Knightly, E. Perahia, and J. Widmer, "IEEE 802.11 ad: Directional 60 Ghz communication for multi-gigabit-per-second wi-fi," *IEEE Commun. Mag.*, vol. 52, no. 12, pp. 132–141, Dec. 2014.

[21] J. Qiao, X. Shen, J. W. Mark, and Y. He, "MAC-layer concurrent beamforming protocol for indoor millimeter-wave networks," *IEEE Trans. Veh. Technol.*, vol. 64, no. 1, pp. 327–338, Jan. 2015.

[22] B.-G. Choi, W.-H. Jeong, and K.-S. Kim, "Characteristics analysis of reflection and transmission according to building materials in the millimeter wave band," *Power (dBm)*, vol. 13, no. 50.62, pp. 64–48, 2015.

[23] W. G. Alliance, "Wigig white paper: Defining the future of multi-gigabit wireless communications," 2010. [Online]. Available: http://wirelessgigabitalliance.org/specifications/

[24] V. Va, J. Choi, and R. W. Heath, "The impact of beamwidth on temporal channel variation in vehicular channels and its implications," *IEEE Trans. Veh. Technol.*, vol. 66, no. 6, pp. 5014–5029, Jun. 2017.

[25] S. N. Chiu, D. Stoyan, W. S. Kendall, and J. Mecke, *Stochastic Geometry and Its Applications*. Hoboken, NJ, USA: Wiley, 2013.

[26] M. Haenggi, *Stochastic Geometry for Wireless Networks*. Cambridge, U.K.: Cambridge Univ. Press, 2012.

[27] K. Venugopal, M. C. Valenti, and R. W. Heath, "Device-to-device millimeter wave communications: Interference, coverage, rate, and finite topologies," *IEEE Trans. Wireless Commun.*, vol. 15, no. 9, pp. 6175–6188, Sep. 2016.
[28] T. Bai, R. Vaze, and R. W. Heath, "Analysis of blockage effects on urban cellular networks," *IEEE Trans. Wireless Commun.*, vol. 13, no. 9, pp. 5070–5083, Sep. 2014.
[29] H. Alzer, "On some inequalities for the incomplete Gamma function," *Math. Comput. Amer. Math. Soc.*, vol. 66, no. 218, pp. 771–778, 1997.

Lan Zhang received the B.E. and M.S. degrees in telecommunication engineering from the University of Electronic Science and Technology of China, Chengdu, China, in 2013 and 2016, respectively. She is currently working toward the Ph.D. degree in the Department of Electrical and Computer Engineering at University of Florida, Gainesville, FL, USA. Her research interests include wireless communications, machine learning, and privacy issues for various cyber-physical systems.

Li Yan received the B.E. degree in communication engineering and the Ph.D. degree in communication and information systems from Southwest Jiaotong University, China, in 2012 and 2018, respectively. She was a Visiting Student at the Department of Electrical and Computer Engineering, University of Florida, Gainesville, FL, USA, from 2017 to 2018. She is currently a Lecturer with Southwest Jiaotong University. Her research interests include 5G communications, mobility managements, network architecture, and HSR wireless communications.

Bin Lin (Member, IEEE) received the B.S. and M.S. degrees from Dalian Maritime University, Dalian, China, in 1999 and 2003, respectively, and the Ph.D. degree from the Broadband Communications Research Group, Department of Electrical and Computer Engineering, University of Waterloo, Waterloo, ON, Canada, in 2009. She is currently a Full Professor and Dean of Communication Engineering Department, School of Information Science and Technology, Dalian Maritime University. She has been a Visiting Scholar with George Washington University, Washington, DC, USA, from 2015 to 2016. Her current research interests include wireless communications, network dimensioning and optimization, resource allocation, artificial intelligence, maritime communication networks, edge/cloud computing, wireless sensor networks, and Internet of Things. Dr. Lin is an Associate Editor of *IET Communications*.

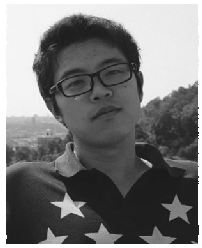

Haichuan Ding received the B.Eng. and M.S. degrees in electrical engineering from the Beijing Institute of Technology (BIT), Beijing, China, in 2011 and 2014, and the Ph.D. degree in electrical and computer engineering from the University of Florida, Gainesville, FL, USA, in 2018. From 2012 to 2014, he was with the Department of Electrical and Computer Engineering, the University of Macau, as a Visiting Student. Since 2019, he has been a Postdoctoral Research Fellow with the Department of Electrical Engineering and Computer Science at the University of Michigan, Ann Arbor, MI, USA. His current research interests include mmWave and V2X communications.

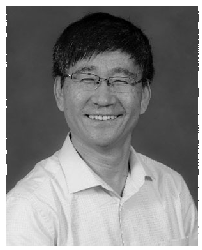

Yuguang Fang (Fellow, IEEE) received the M.S. degree from Qufu Normal University, Shandong, China in 1987, the Ph.D. degree from Case Western Reserve University, in 1994, and the Ph.D. degree from Boston University, in 1997. He joined the Department of Electrical and Computer Engineering at University of Florida in 2000 as an Assistant Professor, then was promoted to Associate Professor, in 2003 and a Full Professor in 2005, and has been a Distinguished Professor since 2019. He holds a University of Florida Foundation Preeminence Term Professorship from 2019–2022, University of Florida Foundation Professorship (2017-2020, 2006-2009), and University of Florida Term Professorship from 2017 to 2021. Dr. Fang received the US NSF Career Award in 2001, the US ONR Young Investigator Award in 2002, the 2019 IEEE Communications Society AHSN Technical Achievement Award, the 2018 IEEE Vehicular Technology Outstanding Service Award, the 2015 IEEE Communications Society CISTC Technical Recognition Award, the 2014 IEEE Communications Society WTC Recognition Award, the Best Paper Award from IEEE ICNP in 2006, and a 2010–2011 UF Doctoral Dissertation Advisor/Mentoring Award. He was the Editor-in-Chief of IEEE TRANSACTIONS ON VEHICULAR TECHNOLOGY from 2013 to 2017 and IEEE WIRELESS COMMUNICATIONS from 2009 to 2012, and serves/served on several editorial boards of premier journals. He also served as the Technical Program Co-Chair of IEEE INFOCOM'2014. He is a fellow of AAAS.

Xuming Fang (Senior Member, IEEE) received the B.E. degree in electrical engineering, the M.E. degree in computer engineering, and the Ph.D. degree in communication engineering from Southwest Jiaotong University, Chengdu, China, in 1984, 1989, and 1999, respectively. He was a Faculty Member with the Department of Electrical Engineering, Tongji University, Shanghai, China, in 1984–1985. He then joined the School of Information Science and Technology, Southwest Jiaotong University, Chengdu, where he has been a Professor since 2001. He held visiting positions with the Institute of Railway Technology, Technical University at Berlin, Berlin, Germany, in 1998–1999, and with the Center for Advanced Telecommunication Systems and Services, University of Texas at Dallas, Richardson, in 2000–2001. He has published more than 200 high-quality research papers in journals and conference publications. He has authored or coauthored five books or textbooks. His research interests include wireless resource management, mmWave communications, and wireless communications for high speed railway. Dr. Fang is the Editor of several journals including IEEE TRANSACTIONS ON VEHICULAR TECHNOLOGY.